Development and Evaluation of a Time-Resolved Near-Infrared Fluorescence Finite Element Model

Qun Zhu*[a], Frederic Leblond[b], Fadi El-Ghussein[b], Brian W Pogue[b] and Hamid Dehghani[a]
[a]School of Computer Science, University of Birmingham, Birmingham, B15 2TT, UK;
[b]Thayer School of Engineering, Dartmouth College, NH 03755, USA.
*q.zhu.1@cs.bham.ac.uk

ABSTRACT

In this work a generalization of the approach allowing time-domain (TD) excitation and fluorescence data to be generated using a finite element model (FEM) is introduced. This new functionality allows simulation of temporal point-spread functions (TPSF) for a heterogeneous scattering and absorbing media of arbitrary geometry. In the first part of this paper, the approach used to develop a computationally efficient model for solving the time-dependent diffusion equation for excitation and fluorescence data is presented. In the second part, a detailed theoretical evaluation of the method is given by comparing the developed FEM simulations with analytical and Monte Carlo data. The total fluence (intensity data), shows qualitative match whereas meantime of flight is almost identical among the three models for both excitation and emission data. The results show that the model is reliable and warrants its use for future TD applications where diffusion modelling can be used.

Keywords: Light propagation in tissues, FEM, Fluorescence, Time-resolved imaging.

1. INTRODUCTION

NIRFAST is an open source software package designed for modeling near infrared (NIR) light transport in biological tissue based on the diffusion equation obtained with a finite element method (FEM). The current version of NIRFAST[1, 2] allows simulations of continuous wave (CW) and frequency domain fluorescence signals for both intrinsic and extrinsic models. In this work we introduce a generalization of the approach allowing time-domain excitation and fluorescence data to be generated. This new functionality allows simulation of temporal point spread functions (TPSF) for heterogeneous scattering and absorbing media of arbitrary geometry.

For clinical applications, this technique can potentially be used to develop a non-invasive *in vivo* molecular imaging technique that not only allows real-time viewing of cellular activity but also is able to extract time related patho-physiological information from biological tissue[3-5]. The technique could be applied for diseases such as cancers detection and diagnosis at a very early stage in comparison with other imaging or detection modalities that require months or years for tumors to grow to be detectable[6-8]. This provides the advantages for faster treatment of the diseases and better therapeutic monitoring and outcomes. In addition, the model in practice could also potentially be used to accelerate drug discovery and development due to it is ability of nearly real-time viewing of cellular activity[3, 9, 10].

Time domain NIR fluorescence imaging is a novel functional imaging technique whereby a region of interest is irradiated by a NIR excitation light source and the emitted fluorescence light together with the transmitted and/or

Optical Tomography and Spectroscopy of Tissue IX,
Edited by Bruce J. Tromberg, Arjun G. Yodh, Mamoru Tamura, Eva M. Sevick-Muraca, Robert R. Alfano,
Proc. of SPIE Vol. 7896, 78960T · © 2011 SPIE · CCC code: 1605-7422/11/$18 · doi: 10.1117/12.873741

reflected light at excitation is used to allow spatial distributions of fluorophores and/or other structures in tissues to be imaged[11-20]. In comparison with the technique being performed using CW and/or in frequency domain[1, 18, 21-26], the time domain technique has shown to provides a more quantitatively accurate results within image reconstruction[27] and particularly from the point of view of spatial resolution. More specifically, since time domain measurement data implicitly contains all modulation frequencies from frequency domain measurement, it should therefore provide much more information regarding the underlying optical properties[28]. Niedre et al[29] have demonstrated that significant resolution improvements in the image reconstructions can be achieved by the use of early photons for fluorescence tomographic imaging of lung tumors in mice *in vivo*. Further studies have also shown that when transmitted through the torso of a mouse, early photons were significantly less diffuse than quasi-cw photons which allowed an improved visualization of fluorescent targets for individual optical projections and reconstructed tomographic images[17]. Leblond et al[16] have also demonstrated that the measurement of early photons allows the improvement of spatial resolution, since it allows the retention of imaging singular modes corresponding to higher spatial frequencies in the image reconstruction problem.

To date, some work relating to time resolved fluorescent modeling has been done; however, they are mostly centered on 2D models[12, 13], and most have been developed for frequency domain systems[24, 25]. The algorithms and techniques presented in this paper are developed for 3D fluorescent models using FEM for time resolved propagation of NIR light. In addition, analytical solutions[15, 18] and Monte Carlo (MC)[20] models have also been used for simulations of 3D fluorescent light propagation in time domain. The analytical solutions provide fast and computationally efficient solutions but suffer from the drawback that they can only be applied for simple homogeneous geometries. The MC models although can be applied for complex geometries, they are very time and computationally expensive to have stable responses[30, 31]. The FEM model introduced in this paper not only can have fast computation but also can be applied for complex heterogeneous geometries.

In the first part of this paper we present the theory used to develop the computationally efficient approach for solving the time-dependent diffusion equation for both excitation and fluorescence data based on FEM. In the second part, a detailed evaluation of the method is presented through comparing FEM numerical simulations with analytical solutions and Monte Carlo simulations.

2. METHOD AND RESULTS

2.1 Theory and Development

The basic theory of the model is the Diffusion Approximation (DA) in time domain. Let the subscripts x and m denote the excitation and emission wavelengths respectively, within a heterogeneous fluorescent turbid medium, Ω which is externally excited by an ideal ultra-short point source (i.e. δ-shaped in space and time). The propagation of both excitation and emission light in the medium can be respectively modeled by the coupled time-domain diffusion equations:

$$\left[\nabla\cdot\kappa_x(r)\nabla-\left(\mu_{ax}(r)+\mu_{afx}(r)\right)c-\frac{\partial}{\partial t}\right]\phi_x(r,r_s,t)=-\delta(r-r_s,t) \tag{1}$$

$$\left[\nabla\cdot\kappa_m(r)\nabla-\mu_{am}(r)c-\frac{\partial}{\partial t}\right]\phi_m(r,r_s,t)=-\frac{\eta(r)}{\tau(r)}c\left[\phi_x(r,r_s,t)\otimes e\left(\tau(r),t\right)\right] \tag{2}$$

where $\phi_v(r, r_s, t)$ $(v \in [x, m])$ is the temporally and spatially varying photon density at time t and position r, corresponding to a δ-shaped source at position r_s; the optical properties involved are the absorption coefficient, $\mu_{av}(r)$ and the diffusion coefficient, $\kappa_v(r, t) = 1/[3(\mu_{av}(r)+\mu'_{sv}(r)]$, where, $\mu'_{sv}(r)$ is the reduced scattering coefficient at the two wavelengths, respectively; the fluorescent parameters are the absorption coefficient of the fluorophore at the excitation wavelength, $\mu_{afx}(r)$, the lifetime, $\tau(r)$, and the quantum efficiency, $\eta(r)$; $e(\tau, t) = e^{-t/\tau}U(t)$ with $U(t)$ being a unit-step function; the operator, $\otimes$, denotes the temporal convolution. In order to more precisely perform the modelling, it should be pointed out that absorption by the fluorophor at the excitation wavelength (i.e. $\mu_{afx}(r)$ in Eq. 1) has to be taken into account as well, since the medium has fluorophore embedded within it.

In order to solve both the excitation (Eq. 1) and emission (Eq. 2) equations at time step k based on FEM, according to the work from Arridge et al[11], Eq. 1 can be derived as:

$$A_x \phi_{x(k+1)} + B_x \phi_{x(k)} = Q_{x(k)}^{(\delta)} \tag{3}$$

which can be re-written as:

$$\begin{cases} A_x \phi_{x(1)} = Q_{x(0)}^{(\delta)} & as\ \phi_{x(0)} = 0 \\ A_x \phi_{x(k+1)} = -B_x \phi_{x(k)} & as\ Q_{x(k)}^{(\delta)} = 0\ when\ k \geq 1 \end{cases} \tag{4}$$

where

$$\begin{aligned} A_x &= \frac{1}{2}K(\kappa) + \frac{1}{2}C(\mu_a c) + \frac{1}{\Delta t}M \\ B_x &= \frac{1}{2}K(\kappa) + \frac{1}{2}C(\mu_a c) - \frac{1}{\Delta t}M \end{aligned} \tag{5}$$

K, C and M are the FEM matrices and Q is the source term, given by:

$$\begin{aligned} K_{ij} &= \int_\Omega \kappa_x(r)\nabla\psi_j(r)\cdot\nabla\psi_i(r)d\Omega \\ C_{ij} &= \int_\Omega \mu_{ax}(r)c\nabla\psi_j(r)\nabla\psi_i(r)d\Omega \\ M_{ij} &= \int_\Omega \psi_j(r)\psi_i(r)d\Omega \\ Q_j(t) &= \int_\Omega \psi_j(r)q_0(r,t)d\Omega \quad (q_0 = \delta - shaped\ source) \end{aligned} \tag{6}$$

where ψ is the basis function and $i, j = 1 \to V$, V is the number of nodes.

Therefore, equivalently in order to model Eq. 1 using FEM, only Eq. 4 needs to be solved, which can be achieved using one Choleski decomposition for A_x followed by one matrix multiplication and one Choleski forward and back substitution per time step. Matrices A_x and B_x are constant throughout the finite differencing procedure. More details about this approach can be referred to the work by Arridge et al[11]. In terms of computational efficiency, the matrix inversion is performed using a bi-conjugate gradient solver with a pre-conditioner based on Choleski factorization only once, which significantly improves the efficiency.

For the emission case, similarly following the deviation for the excitation case, Eq. 2 can be first derived as:

$$A_m \phi_{m(k+1)} + B_m \phi_{m(k)} = Q_{m(k+1)} \tag{7}$$

where

$$\begin{aligned} Q_m(r) &= -\frac{\eta(r)}{\tau(r)} c\left[\phi_x(r, r_s, t) \otimes e^{-t/\tau}\right] \\ &= \left[Q_{m(1)}, Q_{m(2)}, Q_{m(3)}, \cdots, Q_{m(k)}\right] \end{aligned} \tag{8}$$

Similar to Eq. 4, Eq. 7 can be then re-written as

$$\begin{cases} A_m \phi_{m(1)} = Q_{m(1)} & as\ \phi_{m(0)} = 0, \quad k = 0 \\ A_m \phi_{m(k+1)} = Q_{m(k+1)} - B_m \phi_{m(k)} & k \geq 1 \end{cases} \tag{9}$$

where A_m and B_m are the same as those generated from Eq. 5 except with the optical properties (μ_{am}, μ_{sm} and μ_{afx}) used are in the emission wavelength (i.e. fluorophore sources) rather than in the excitation wavelength. In terms of solving Eq. 9, the same method that is applied for solving Eq. 4 can be used. Therefore, by following the same process that applied to model the excitation light, the propagation of emission light in time domain which is modeled by using FEM can be achieved. Additionally, the same Cholesky factorization that is used as a pre-conditioner for the excitation part can also be used for the emission case, further reducing the computational complexity.

The main different difference between the two equations (Eq. 4 and Eq. 9) is the source term on the right hand side. For the excitation case, it is simply the δ function while it is more complex for the emission case which depends not only on the fluorescent properties but also depends on the spatially variant excitation light. In terms of performing the modeling in time domain, for the excitation, the first time step intensity ($\phi_{x(1)}$) can be obtained by solving the Eq. 4 with the δ source and then the calculated solution at $k = 0$, is used as the source term for calculating the intensity in the next time step by solving Eq.4 again. This process will be repeated for the intensity calculations for the rest of the time steps until the end of the length of modeling time. For the emission case, the first time step intensity $\phi_{m(1)}$ can be obtained by solving Eq. 9 with the convolution of $\phi_{x(1)}$ and τ as the source term which also depends on η. The next time step intensity $\phi_{m(2)}$ can also be generated by solving Eq. 2 again but with the source term depending on η, $\phi_{m(1)}$ and the convolution of $\phi_{x(2)}$ and τ. The rest of the time step intensity $\phi_{m(k)}$ *(k=3, 4, 5⋯)* can be then obtained by following the same process for generating $\phi_{m(2)}$ until the end of the modeling time.

In order to obtain the TPSFs (i.e. ϕ_v) of the excitation and emission using the FEM model, firstly, the medium of interest has to be modelled and discretised appropriately for the application of FEM; secondly, the FEM matrices (A_v and B_v) have to be developed, followed by one Choleski calculation to solve Eq. 4 and Eq. 9. More details about the FEM model of obtaining the intensities of both excitation and emission for all the time steps can be illustrated by a pseudo algorithm as follows:

```
load the mesh of medium;
calculate the FEM matrices (A_v and B_v);
generate the source matrix for excitation (Q_x) for multi sources;
for all sources
```

```
If the excitation pre-conditioner (R_x) exist;
  No Calculate R_x based on Choleski factorization;
  Yes continue;
end
time step k = 1;
solve Eq. 4 for φ_x(1) using a bi-conjugate gradient solver with A_x, Q_x and R_x;
time step k > 1;
solve Eq. 4 for φ_x(k) using a bi-conjugate gradient solver with A_x, B_x and R_x;
generate the source matrix for emission (Q_m) based on φ_x, η and τ (i.e. Eq. 8);
time step k = 1;
solve Eq. 9 for φ_m(1) using a bi-conjugate gradient solver with A_m, Q_m(1) and R_m;
time step k > 1;
solve Eq. 9 for φ_m(k) using a bi-conjugate gradient solver with A_m, B_m, Q_m(k) and R_m;
end
```

2.2 Theoretical Evaluation

In order to evaluate the FEM model, we have used both an analytical solution and a Monte Carlo (MC) model. This includes two parts; one performs the comparison of the TPSFs of both the excitation and emission on the same model calculated using the FEM and the analytical implementation respectively. The other one performs the same comparison on another model but using not only both the FEM and the analytical solution but also the MC model as well. In addition, the comparisons of TPSF data-types including total light fluence (intensity), mean-time of photon arrival and fluorescence to transmission ratio against source/detector distances on the same model are also presented. In all cases, a semi-infinite model was assumed for the analytical and MC solution and a 3D slab geometry for the FEM solution, with the measurements taken as the reflectance measurements as a function of distance from the source. The optical and physical properties of the two separate physical models used for comparisons are shown in Table 1.

Table 1: Optical and physical properties of the media used for the modelling evaluation.

	Model 1	Model 2
$\mu_{ax} = \mu_{am}$	0.0015 mm^{-1}	0.035 mm^{-1}
$\mu_{sx} = \mu_{sm}$	30 mm^{-1}	10 mm^{-1}
$g_x = g_m$	0.8	0.9
$\mu_{sx}' = (1-g_x)\,\mu_{sx}$	6 mm^{-1}	1 mm^{-1}
$\mu_{sm}' = (1-g_m)\,\mu_{sm}$	6 mm^{-1}	1 mm^{-1}
τ	1 ns	2.8 ns
η	0.15	0.1
μ_{afx}	0.001 mm^{-1}	0.01 mm^{-1}
Refractive index (n)	1.44	1.33
Detector	1, 3, 5, 10, 15 and 26 mm from the source	
Source	(0, 0, 0)	
mesh resolution: x	-50:1:85 mm	-50:0.85:85 mm
mesh resolution: y	0:1:40 mm	0:0.85:40 mm
mesh resolution: z	-30:1:30 mm	-30:0.85:30 mm
dt	40 ps	20 ps
t	40 ns	40 ns

μ_{av} is the absorption coefficient, μ_{sv} is the scattering coefficient, g_v is the scattering anisotropy factor and μ_{sv}' is the reduced scattering coefficient at excitation (v = x) and emission (v = m) wavelengths respectively. μ_{afv} is the absorption coefficient of the fluorophore at excitation (v = x). η is the fluorophore quantum efficiency which in together with lift-time (τ) represents the ability of the fluorophore of generating fluorescent light. n is the refractive index and t and dt are the total time used for each TPSF acquisition and the time step respectively. x, y and z specify the dimensions of the fluorescent slab model used for the FEM mesh.

2.2.1. Comparison with analytical solution on model 1

In order to evaluate the FEM model, the comparisons with an analytical model on the excitation and emission TPSFs of model 1 shown in Table 1 is considered. The analytical model that has been used is briefly introduced first and more details about the model can be found in the work from Patterson and Pogue[18].

The excitation and emission light modelling are given respectively as:

$$R_x(\rho,t) = \frac{z_0}{(4\pi Dc)^{3/2}} t^{-5/2} \exp\left(-\frac{\rho^2+z_0^2}{4Dct}\right)\exp(-\beta_x t) \tag{10}$$

$$R_m(\rho,t) = F_{xm}(\rho,t) \otimes \frac{1}{\tau}\exp\left(-t/\tau\right) \tag{11}$$

where

$$\begin{aligned} F_{xm}(\rho,t) = {} & \frac{\mu_{fx}\eta c z_0}{(4\pi Dc)^{3/2}(\beta_x-\beta_m)} t^{-5/2} \\ & \times \exp\left(-\frac{\rho^2+z_0^2}{4Dct}\right)\left[\exp(-\beta_m t)-\exp(-\beta_x t)\right] \end{aligned} \tag{12}$$

$$\begin{aligned} \beta_x &= c(\mu_{ax}+\mu_{fx}) \\ \beta_m &= c(\mu_{am}+\mu_{fm}) \end{aligned} \tag{13}$$

$$z_0 = \frac{1}{\mu_s(1-g)} \tag{14}$$

$$D \cong \frac{1}{3\mu_s(1-g)} \tag{15}$$

where μ_{fx} and μ_{fm} are the absorption coefficients of fluorophore at the excitation and emission wavelength respectively. η is the quantum efficiency of fluorophore. c is the speed of light in the medium. ρ is the detection position on the boundary from the source. The other parameters are the same as those described in Table 1. As the Eqs. 10-15 show, the analytical solutions for the excitation and emission cases are similar except the fluorescent properties (lifetime in form of the convolution of the fluorophore absorption and fluorescent quantum efficiency) which are taken into account in the emission case. These are similar to the FEM solutions which provide initial consistence with the numerical approach taken.

After performing both the FEM and analytical simulations on model 1, the calculated TPSFs of the excitation and emission at detectors 4 and 6 are shown in figure 1(a) and 1(b) respectively, which are normalized to the maximum value. As the result shows, it can be seen that all the TPSF responses vary with time with the responses at detector 4 decaying faster than those at detector 6, as expected. In addition, the excitation responses are always leading the emission responses for both detector cases. Finally the figure clearly shows that both the excitation and emission responses generated using the FEM and analytical models match very well to each other at both detectors, which initially validates that the FEM model is accurate and reliable. The number of FEM nodes and linear tetrahedral elements for model 1 are 340136 and 1944000 respectively. The running time taken by the FEM model is 54.22 minutes by using a PC with six-core ×2.2GHz AMD Opteron(tm) Processor 2427, with no parallelisation.

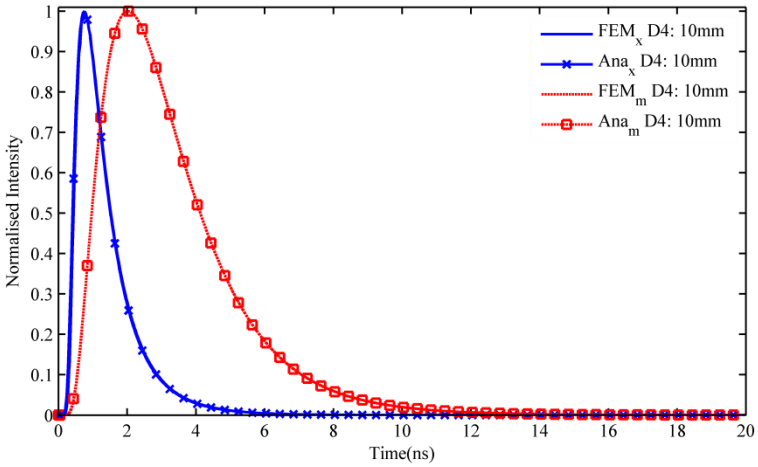

(a)

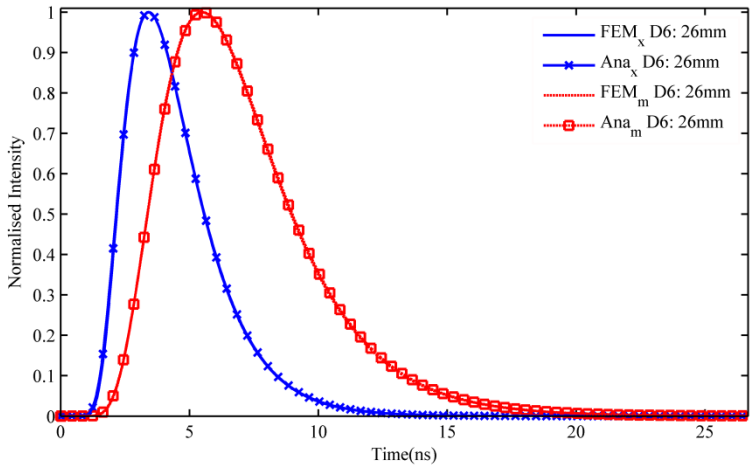

(b)

Figure 1. Comparison of TPSFs from FEM (lines without marker) and analytical (lines with marker) simulations on model1. Solid-blue and dashed-red lines: excitation and emission respectively with the detector located at (a) 10mm and (b) 26mm away from the source.

2.2.2. Comparison with analytical and MC simulations on model 2

In order to further evaluate the FEM model another comparison of TPSFs of excitation and emission on model 2 whose physical and optical properties were shown in Table 1 is presented. The TPSFs are generated respectively using not only the FEM and the analytical models but also the MC[20] model as well. The MC model is able to produce the TPSFs of the

excitation and emission from a fluorescent turbid medium; however, it is a statistical approach rather than a FEM method, which normally requires a large number of photons to be run and hence requires more time to have efficient results. Details of the algorithm can be referred to the work of Vishwanath and Mycek[20]. The MC model is applied as it does not rely on diffusion approximation and is considered as the gold standard. With $2x10^9$ photons being run in the MC simulation, the comparing TPSF results of the excitation and emission on model 2 at the same detectors as those shown in figure 1 are shown in figure 2(a) and 2(b) respectively. The number of FEM nodes and linear tetrahedral elements for model 2 are 461208 and 2645954 respectively. By using the same computer as described early, the running time taken by the FEM model is 192.28 minutes (3.2 hours), by the MC model is 16348.38 minutes (11.35 days) and by the analytical model is 5.95×10^{-4} minute (0.036 seconds).

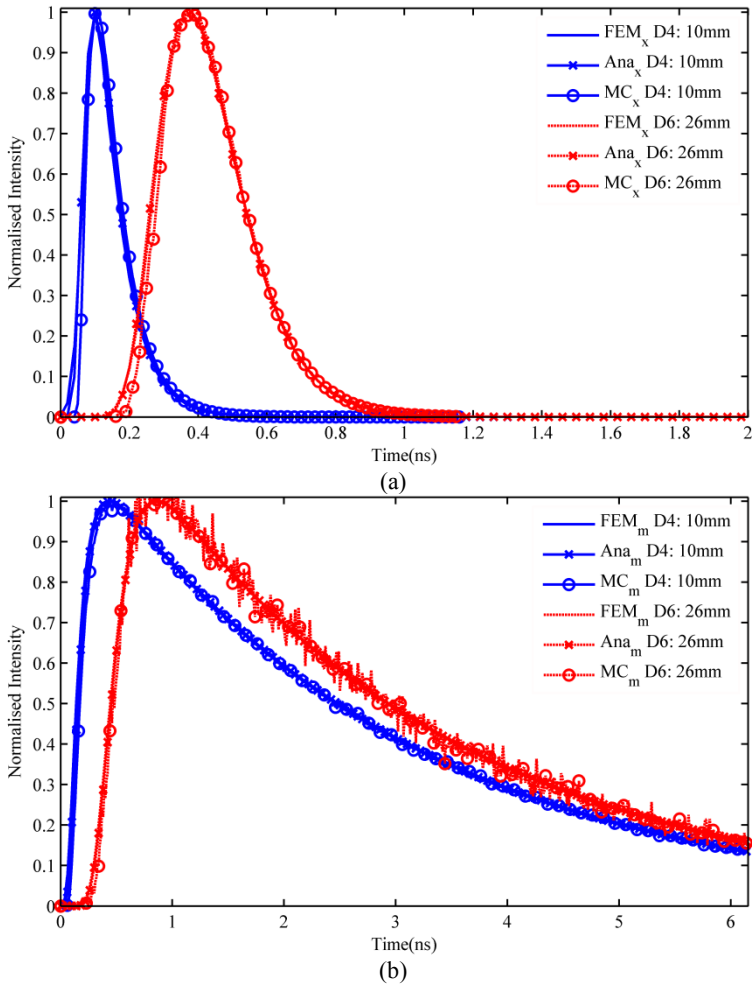

Figure 2. Comparison of TPSFs from FEM (lines without marker), analytical (lines with cross) and MC (lines with circle) simulations on model2 for excitation (a) and emission (b). Solid-blue lines: detector located at 10mm away from the source; dashed-red lines: detector at 26mm.

The TPSFs shown in figure 2 are normalized respectively to their maximum. The overall results of both the excitation and emission cases generated from the three models at both the detectors match well to each other. This further provides evidence that the FEM model based data is reliable. The small discrepancy shown at the early time in figure 2(a) is due to the diffusion approximation equation that is for the FEM and analytical solution is not accurate for early photons. This discrepancy exist is figure 2(b) as well although it is not clearly evident due to the scale of the axis. The MC TPSF of the

emission cases at the both detectors become noisy as there are not enough fluorescent photons being generated as the medium is highly absorbing with low quantum efficiency. The data from detector at 26 mm is noisier since the detector is too far from the source and hence less photons can reach the detector. This noise can be reduced by simulating more photons; however, more computation time will be needed.

To further perform the evaluation, the comparisons of TPSF data-types which include total light fluence (intensity), mean-time of photon arrival and fluorescence to transmission ratio against source/detector distances on model 2 are presented in figures 3-5 respectively.

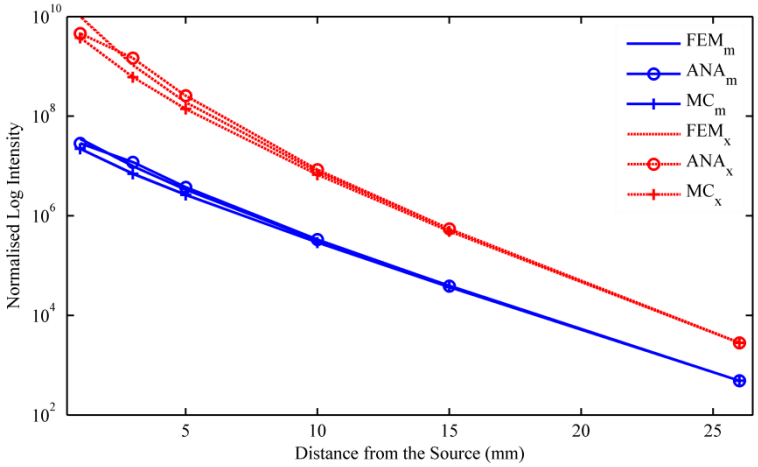

Figure 3. Normalised intensity in log of excitation (dashed-red) and emission (solid-blue) on model 2 simulated by the FEM model (lines without marker), the analytical solution (lines with circle marker) and the MC model (lines with plus marker) at varying source/detector distances of 1mm to 26mm.

Figure 3 shows the comparison of the calculated total intensity (i.e. the integration of the TPSF) among the three models (FEM, analytical and MC) as a function of varying distance away from the source from 1 mm to 26 mm for both excitation and emission data respectively. The curves are normalised to the values of the MC TPSFs at 26 mm as the MC model does not rely on diffusion approximation and is considered as the gold standard. As shown, overall both the excitation and emission cases among the three methods applied show good agreements. As expected, they all reduce in an almost linear fashion with respect to increasing distance except for the variation between 1 mm to 10 mm, where the difference of the FEM with respect to the MC data decrease from 62.43% to 12.77% for the excitation case and from 36.74% to 10.16% for the emission case. The same differences between the FEM and analytical simulations are smaller, which are from 54.33% to 9.47% and 18.53% to 3.42% respectively. The differences are caused by in fact that the diffusion approximation (DA) equation that is the basis for the FEM and analytical solution is not accurate for early photons and small distance simulations. However, the smaller differences between the FEM and analytical simulations, which are both based on DA can be due to the different models of the source implementation.

Figure 4 shows the comparisons of mean-time of photon arrival among the three methods applied with varying with distance away from the source from 1 mm to 26 mm for both excitation and emission data respectively. As shown, the mean-time of photon arrivals taken in the emission cases are longer than those in the excitation cases, which are expected and consistent with those shown in figure 2. In addition, also as expected, the mean-time of flight is linear with respect to distance away from the source. In general, a good match (almost identical) is seen among the measured values from the three models, which indicate the FEM model is well developed.

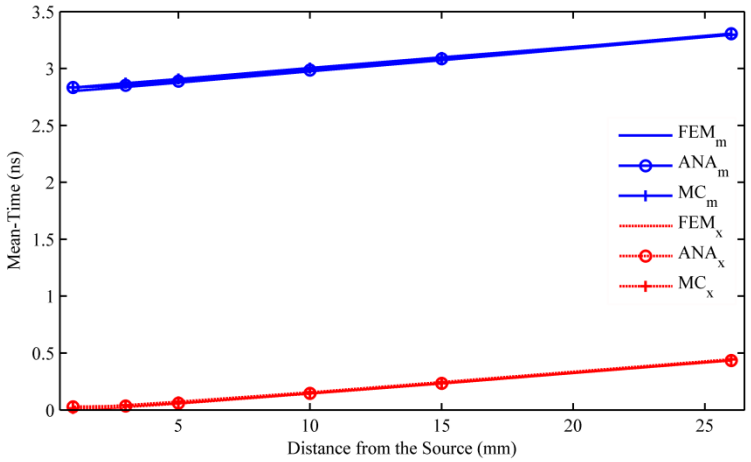

Figure 4. Mean-time of excitation (dashed-red) and emission (solid-blue) on model 2 simulated by the FEM model (lines without marker), the analytical solution (lines with circle marker) and the MC model (lines with plus marker) at the distance away from the source from 1mm to 26mm.

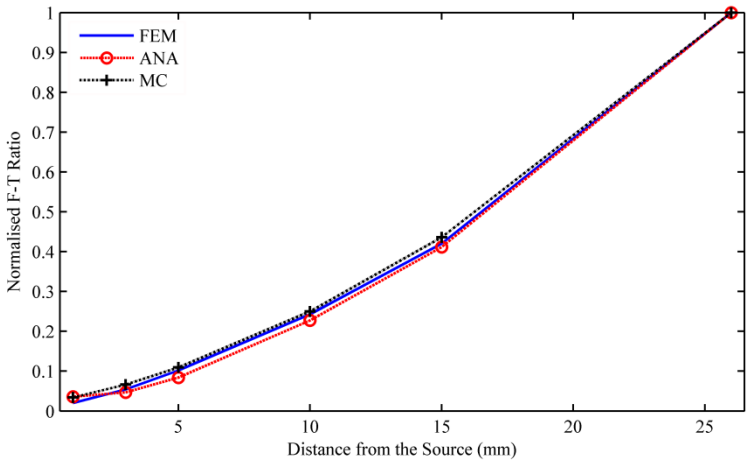

Figure 5. Normalised fluorescent to transmission ratio for the FEM model (solid-blue), the analytical solution (dash-circle-red) and the MC simulations (dashed-dot-plus-black) varying with the distance away from the source from 1mm to 26mm on model 2.

Figure 5 shows the fluorescent to transmission ratio of the intensity data measured by the three models, varying with the distance away from the source from 1 mm to 26 mm. This is obtained directly from the division of the emission intensity to the excitation intensity and it is normalised. In general, the figure shows good match in terms of the variation tends to increase with distance increases for all the cases. They are varying in the same trend, the lines from FEM and analytical solutions are almost overlapped to each other. The largest difference, which is calculated the same as that calculated for figure 3, between the FEM and MC is 17.48% at the distance of 5 mm.

3. DISCUSSION AND CONCLUSION

In this paper, the FEM implementation of the time resolved (TR) fluorescence light propagation in soft tissue based on the diffusion approximation has been developed and has been evaluated using both analytical and Monte Carlo (MC) simulation. Using the analytical solution for the TR model based on a semi-infinite medium, the data using a 3D FEM model was evaluated and shown to provide an excellent match (figure 1). The data presented were for two separate

source and detector distance for reflectance measurements for a given set of optical properties, Table 1, and although not shown, similar results were found for varying optical parameters.

Acknowledging the fact that both the analytical and FEM solutions are based on the diffusion approximation, a MC model was also utilised to provide additional tools for the evaluation of both the FEM and the analytical solution, figures 2-5. It is seen that TPSFs and its data-types (intensity and mean-time) generated for both the excitation and emission light propagation, due to a homogenous model (Table 1) provide a good match between all different (FEM, analytical and MC) simulations. It is evident from figures 2 and 3, that the FEM and analytical solutions do not model the early photon propagation, due to the utilisation of the diffusion approximation. Nonetheless, the overall agreement for the TPSF (figure 2) and its data-types (figures 3 and 4) among these three different models is found to be good in terms of the expected shape and responses. The TPSF data from the MC model show the inherent noise as a function of large source/detector separation in the emission data, which can be overcome with a larger number of simulated photons, which highlights the limitation of using probabilistic methods for TR light propagation models. Although not shown, the effect of the noise in MC generated TPSF is more profound for models of higher absorption and even larger source/detector separation. Finally, in order to provide a direct comparison between the ratio of the normalised fluorescent to transmission data (emission versus excitation); figure 5 demonstrates good qualitative and quantitative accuracy of the FEM model versus the analytical and MC data.

In conclusion, a 3D FEM based diffuse TR model for near-infrared light transport in biological tissue has been presented. This new functionality allows simulation of both excitation and fluorescence TPSFs for heterogeneous scattering and absorbing media of arbitrary geometry. The paper focuses on the development and valuations of the model. The evaluations are performed theoretically via comparisons with analytical and MC simulations. It has been demonstrated that the use of intensity only data may provide inaccuracies, unless the power of the excitation source can be adequately accounted for, whereas the mean-time or variance of the data can provide a much more accurate representation. This work allows a direct mechanism to further evaluate and investigate the use of different time-bins to improve both the quantitative and qualitative accuracy of molecular fluorescence imaging.

ACKNOWLEDGMENT

This work has been funded by the National Institutes of Health (NIH) grants R01CA132750, RO1CA120368 and K25 CA138578 through the National Cancer Institute (NCI).

REFERENCES

[1] Dehghani, H., Eames, M. E., Yalavarthy, P. K., Davis, S. C., Srinivasan, S., Carpenter, C. M., Pogue, B. W., and Paulsen, K. D., "Near Infrared Optical Tomography using NIRFAST: Algorithms for Numerical Model and Image Reconstruction Algorithms," Communications in Numerical Methods in Engineering, (2009, DOI: 10.1002/cnm.1162).

[2] "NIRFAST" (Dartmouth College), retrieved www.nirfast.org.

[3] Luker, G. D. and Luker, K. E., "Optical Imaging: Current Applications and Future Directions," The Journal of Nuclear Medicine 49(1), 1-4 (2008).

[4] Zhang, L., Lee, K. C., Bhojani, M. S., Khan, A. P., Shilman, A., Holland, E. C., Ross, B. D., and Rehemtulla, A., "Molecular imaging of AKT kinase activity," Nat Med 13(9), 1114 - 1119 (2007).

[5] Massoud, T. F., Paulmurugan, R., and Gambhir, S., S., "Molecular imaging of homodimeric protein-protein interactions in living subjects," The FASEB Journal 18(10), 1105-1107 (2004).

[6] Palmedo, H., Hensel, J., Reinhardt, M., Von Mallek, D., Matthies, A., and Biersack, H. J., "Breast cancer imaging with PET and SPECT agents: an in vivo comparison," Nucl. Med. Biol. 29(8), 809-815 (2002).

[7] Houston, S. T., Jones, L. W., and Waluch, V., "Nuclear magnetic resonance imaging in detecting and staging prostatic cancer," Urology 31(2), 171-175 (1988).

[8] Warner, E., Plewes, D. B., Shumak, R. S., Catzavelos, G. C., Di Prospero, L. S., Yaffe, M. J., Goel, V., Ramsay, E., Chart, P. L., Cole, D. E. C., Taylor, G. A., Cutrara, M., Samuels, T. H., Murphy, J. P., Murphy, J. M., and Narod, S. A., "Comparison of Breast Magnetic Resonance Imaging, Mammography, and Ultrasound for Surveillance of Women at High Risk for Hereditary Breast Cancer," Journal of Clinical Oncology 19(15), 3524-3531 (2001).

[9] Rudin, M. and Weissleder, R., "Molecular imaging in drug discovery and development," Nat Rev Drug Discov 2(2), 123–131 (2003).

[10] Gross, S. and Piwnica-Worms, D., "Molecular imaging strategies for drug discovery and development," Current Opinion in Chemical Biology 10(4), 334-342 (2006).

[11] Arridge, S. R., Schweiger, M., Hiraoka, M., and Delpy, D. T., "A finate element approach for modeling photon transport in tissue," Medical Physics 20(2), 299-309 (1993).

[12] Gao, F., Zhao, H. J., Tanikawa, Y., and Yamada, Y., "A linear, featured-data scheme for image reconstruction in time-domain fluorescence molecular tomography," Optics Express 14(16), 7109-7124 (2006).

[13] Gao, F., Zhao, H. J., Zhang, L. M., Tanikawa, Y., Maejono, A., and Yamada, Y., "A self-normalized, full time-resolved method for fluorescence diffuse optical tomography," Optics Express 16(17), 13104-13121 (2008).

[14] Kumar, A. T. N., Raymond, S. B., Boverman, G., Boas, D. A., and Bacskai, B. J., "Time-resolved fluorescence tomography of turbid media based on lifetime contrast," Optics Express 14(25), 12255-12270 (2006).

[15] Lam, S., Lesage, F., and Intes X, X., "Time-domain fluorescent diffuse optical tomography: analytical expressions," Optics Express 13(7), 2267-2275 (2005).

[16] Leblond, F., Dehghani, H., Kepshire, D., and Pogue, B. W., "Early-photon fluorescence tomography: spatial resolution improvements and noise stability considerations," Journal of the Optical Society of America A 26(6), 1444-1457 (2009).

[17] Niedre, M. and Ntziachristos, V., "Comparison of fluorescence tomographic imaging in mice with early-arriving and quasi-continuous-wave photons," Optics Letters 35(3), 369-371 (2010).

[18] Patterson, M. S. and Pogue, B. W., "Mathematical model for time-resolved and frequency-domain fluorescence spectroscopy in biological tissues," Applied Optics 33(10), 1963-1974 (1994).

[19] Soloviev, S. V., Tahir, K. B., McGinty, J., Elson, D. S., Neil, M. A. A., French, P. M. W., and Arridge, S. R., "Fluorescence lifetime imaging by using time-gate data," Applied Optics 46(30), 7384-7391 (2007).

[20] Vishwanath, K. and Mycek, M. A., "Time-resolved photon migration in bi-layered tissue models," Optics Express 13(19), 7466-7482 (2005).

[21] Dehghani, H., Davis, S. C., Jiang, S. D., Pogue, B. W., Paulsen, K., and Patterson, M., "Spectrally-Resolved Bioluminescence Optical Tomography," Optics Letters 31(3), 365-367 (2006).

[22] Dehghani, H., Srinivasan, S., Pogue, B. W., and Gibson, A., "Numerical modelling and image reconstruction in diffuse optical tomography," Phil. Trans. R. Soc. A 367(1900), 3073-3093 (2009).

[23] Dehghani, H., White, B. R., Zeff, B. W., Tizzard, A., and Culver, J. P., "Depth sensitivity and image reconstruction analysis of dense imaging arrays for mapping brain function with diffuse optical tomography," Applied Optics 48(10), D137-D143 (2009).

[24] Jiang, H., "Frequency-domain fluorescent dissusion tomography: a finite-element-based algorithm and siulation," Applied Optics 37(22), 5337-5343 (1998).

[25] Lee, J. and Sevick-Muraca, E. M., "Three-dimensional fluorescence enhanced optical tomography using referenced frequency-domain photon migration measurements at emission and excitation wavelengths," Journal of the Optical Society of America A 19(4), 759-771 (2002).

[26] Milstein, A. B., Stott, J. J., Oh, S., Boas, D. A., Millane, R. P., Bouman, C. A., and Webb, K. J., "Fluorescence optical diffusion tomography using multiple-frequency data " J. Opt. Soc. Am. A 21(6), 1035-1049 (2004).

[27] Keren, S., Gheysens, O., Levin, C. S., and Gambhir, S. S., "A comparison between a time domain and continuous wave small animal optical imaging system," IEEE Trans Med Imaging 27(1), 58-63 (2008).

[28] Marjono, A., Yano, A., Okawa, S., Gao, F., and Yamada, Y., "Total light approach of time-domain fluorescence diffuse optical tomography," Optics Express 16(19), 15268-15285 (2008).

[29] Niedre, M. J., de Kleine, R., Aikawa, E., Kirsch, D. G., Weissleder, R., and Ntziachristos, V., "Early photon tomography allows fluorescence detection of lung carcinomas and disease progression in mice in vivo," Proc. Natl. Acad. Sci. U.S.A. 105(49), 19126–19131 (2008).

[30] Preisa, T., Virnaua, P., Paula, W., and Schneidera, J. J., "GPU accelerated Monte Carlo simulation of the 2D and 3D Ising model," Journal of Computational Physics 228(12), 4468-4477 (2009).

[31] Fang, Q. Q. and Boas, D. A., "Monte Carlo simulation of photon migration in 3D turbid media accelerated by graphics processing units," Optics Express 17(22), 20178-20190 (2009).